Published by IOP Publishing for Sissa Medialab

Received: *February 14, 2020*
Accepted: *April 24, 2020*
Published: *June 1, 2020*

Coincidence time resolution investigation of BaF_2-based H6610 detectors for a digital positron annihilation lifetime spectrometer

R. Ye, Q.H. Zhao, H.B. Wang, B.C. Gu, Z.W. Pan, J.D. Liu and B.J. Ye[1]

State Key Laboratory of Particle Detection and Electronics,
University of Science and Technology of China,
Hefei 230026, China

E-mail: bjye@ustc.edu.cn

Abstract: BaF_2-based detectors have been used in many fields requiring fast timing, especially in positron annihilation lifetime (PAL) spectroscopy. The performance of a PAL spectrometer is closely correlated with the time response of BaF_2-based detectors. Therefore, it is important to select scintillation detectors with excellent time resolution. In this work, the coincidence time resolution of BaF_2-based H6610 detectors was investigated using a digital oscilloscope. The time response of detectors has been optimized by tuning the supply voltages, the sampling rate of the oscilloscope, and digital fraction constants, achieving a conicidence time resolution of about 162 ps for the 0.511 MeV annihilation γ-ray pairs and 108 ps for the ^{60}Co cascade γ-rays, respectively. Furthermore, a digital PAL spectrometer composed of two BaF_2-based H6610 detectors and an oscilloscope was developed with a time resolution of around 130 ps, much better than most digital PAL spectrometers.

Keywords: Gamma detectors (scintillators, CZT, HPGe, HgI etc); Timing detectors; Data processing methods; Detection of defects

[1]Corresponding author.

https://doi.org/10.1088/1748-0221/15/06/P06001

2020 JINST 15 P06001

Contents

1 Introduction

BaF_2 crystal is known as one of the fastest inorganic scintillators at present, which has a fast scintillation component with a decay time around 600–800 ps [1, 2]. Therefore, BaF_2-based scintillation detectors have attracted considerable attention. They are widely used in several fields requiring fast timing, such as time-of-flight positron emission tomography [3], hard X-ray imaging [4], neutron radiation capture cross section measurements [5], lifetime measurements of nuclear excited states [6], and positron annihilation lifetime (PAL) spectroscopy [7, 8].

PAL spectroscopy has turned out to be a unique method to investigate the microstructures of condensed materials, especially vacancy-type defects and open volume defects [9, 10]. In general, materials like metals and alloys have short lifetime components (less than 200 ps) due to the high electron density. Vacancies or vacancy clusters in materals lead to the longer lifetime up to several hundred picoseconds [11]. Moreover, the lifetime reaches nanosecond level (1–142 ns) in the materials with voids owing to the ortho-positronium (o-Ps) formation on the surface of voids. In the voids, the so-called pick-off annihitation of o-Ps [12], in which the positron in o-Ps annihilates with an electron of antiparallel spin from the surroundings, is superior to self-annihilation [13]. The lifetime value depends on the size of the void [14]. The "lifetimes" between the implanting and annihilating of positrons in samples can be measured using a PAL spectrometer. The conventional PAL spectrometer consists of a pair of scintillation detectors and some NIM standard electric modules including constant fraction differential discriminator (CFDD), time-to-amplitude converter (TAC), and multi-channel analyzer (MCA). Time resolution is considered as one of the key parameters to evaluate the characteristics of a PAL spectrometer. Numerous efforts have been made to improve the time resolution of PAL spectrometers over the past twenty years [15–26]. The tendency is to develop digital PAL spectrometers in which analog electric modules are substituted by fast digitizers. Digital spectrometers have advantages in data processing capability and time performance compared to the

2020 JINST 15 P06001

conventional ones. Several digital PAL spectrometers with time resolution around 140–200 ps in FWHM (full width at half maximum) have been developed [16, 19, 22, 23, 26]. Generally speaking, the performance of a digital PAL spectrometer depends not only on state-of-the-art digitizers and appropriate data processing algorithms but also on fast scintillators and photomultiplier tubes (PMTs). Therefore, it is also critical to select excellent PMTs for digital spectrometers. Photonis XP2020Q and Hamamatsu H3378 PMTs are commonly used in most PAL spectrometers, and the time performances of corresponding scintillation detectors have been investigated comprehensively. However, Hamamatsu H6610 PMTs (faster time response than H3378 PMTs) are rarely applied in PAL spectrometers.

In this work, we investigated the time performance of BaF_2-based H6610 detectors which are composed of Hamamatsu H6610 PMTs and BaF_2 scintillators via a fast digital oscilloscope. The time response of detectors has been optimized by tuning several parameters. Moreover, a new digital PAL spectrometer was developed using two BaF_2-based H6610 detectors and a digital oscilloscope, achieving the best time resolution of about 130 ps. The time response of BaF_2-based H3378 detectors was also discussed for comparison.

2 Experimental setup and methods

2.1 Detector

As shown in figure 1, the dimensions of BaF_2 scintillators (from Beijing Scitlion Technology Corp., Ltd.) were equal to $\Phi 40 \times 25$ mm (as reference) and $\Phi 20 \times 15$ mm, respectively. The surfaces of BaF_2 scintillators were polished to obtain good optical quality. The Hamamatsu H6610 and H3378 PMTs (from Hamamatsu Photonics K.K.) are both of the subnanosecond time response. The typical characteristics of H3378 and H6610 PMTs [27–29] are shown in table 1. Compared to H3378 PMT, H6610 PMT has a smaller effective area, shorter transit time and transit time spread, lower supply voltage, and higher gain. The $\Phi 20 \times 15$ mm BaF_2 scintillators were wrapped with Teflon tapes, leaving the bottom surfaces to mount on H6610 PMTs. BaF_2-based H6610 detectors were composed of $\Phi 20 \times 15$ mm BaF_2 scintillators coupled to H6610 PMTs with DC200 silicone grease. As reference detectors, the $\Phi 20 \times 15$ mm BaF_2 scintillators were also mounted on H3378 PMTs, which were marked as BaF_2-based H3378 detectors. A pair of scintillation detectors (detector-A and detector-B) for each type were utilized in the following experiments.

Table 1. The typical characteristics of Hamamatsu H3378 and H6610 PMTs.

PMT	Effective area (mm)	Rise time (ns)	Transit time (ns)	Transit time spread (ns)	Maximum supply voltage (V)	Gain	Spectral response (nm)
H3378	46	0.7	16	0.37	3500	2.5×10^6	160–650
H6610	20	0.7	10	0.16	2500	5.7×10^6	160–650

2.2 Coincidence time resolution measurement system

As shown in figure 2 (a), the coincidence time resolution (CTR) measurement system was configured. Detector-A and detector-B were in face-to-face geometry. A ^{22}Na source of about 0.37 MBq

2020 JINST 15 P06001

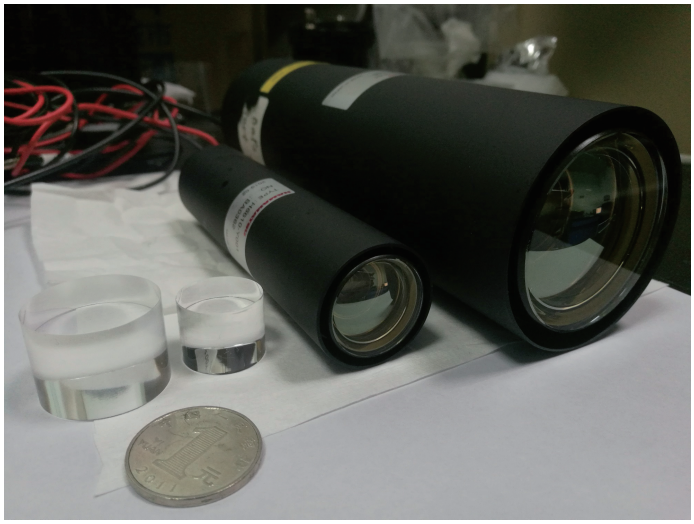

Figure 1. (Left to right) $\Phi 40 \times 25$ mm BaF_2 scintillator, $\Phi 20 \times 15$ mm BaF_2 scintillator, Hamamatsu H6610 PMT, and Hamamatsu H3378 PMT.

was sandwiched between two identical samples, which were marked as ^{22}Na source-sample. The ^{22}Na source-sample was inserted between the two detetors. The 0.511 MeV annihilation γ-ray pairs from the ^{22}Na source-sample were detected by the detectors. The anode pulses of the detectors were led to a digital oscilloscope (LeCroy HDO9204), which has 4 channel inputs, an analog bandwidth of 2 GHz, and the maximum 40 GS/s sampling rate on 2 channels. For the trigger condition, we used the pattem trigger mode and set the trigger threshold of each channel to an appropriate value according to the amplitude of the pulse. Once the trigger condition was satisfied, the waveforms shown on the oscilloscope screen were considered as coincidence events. They were recorded in digital and stored in a portable hard drive connected to the oscilloscope. Then the waveform data were transferred to a PC for further analysis. We used ROOT [30] and GNU Scientific Library [31] to analyze the waveform data and rebuilt the time spectrum for 0.511 MeV annihilation photons.

In the experimental process, a series of high voltages were applied on the detectors. For the waveform data at each kind of voltage setting, we used different constant fraction values (see section 2.5) varied from 0.1 to 0.6 in the timing analysis to obtain the minimum value of time resolution. In this way, the high voltage setting and constant fraction were optimized. The obtained high voltage setting was applied in forthcoming experiments, and the constant fraction was used in the timing analysis of stop signals (from 0.511 MeV γ-rays) for the digital PAL spectrometer (see section 2.3).

As shown in figure 2 (b), we replaced the ^{22}Na source-sample with a ^{60}Co source. The 1.17 and 1.33 MeV γ-rays produced from the decay of ^{60}Co source were detected by the detectors. A similar data acquisition method was applied to obtain the time spectrum for the ^{60}Co cascade radiations. As the energy of the γ-rays from ^{60}Co is approximate to that of 1.275 MeV γ-rays, the optimal constant fraction value obtained from the time spectrum for the ^{60}Co cascade radiations was used in the timing analysis of start signals (from 1.275 MeV γ-rays) for the digital PAL spectrometer.

2020 JINST 15 P06001

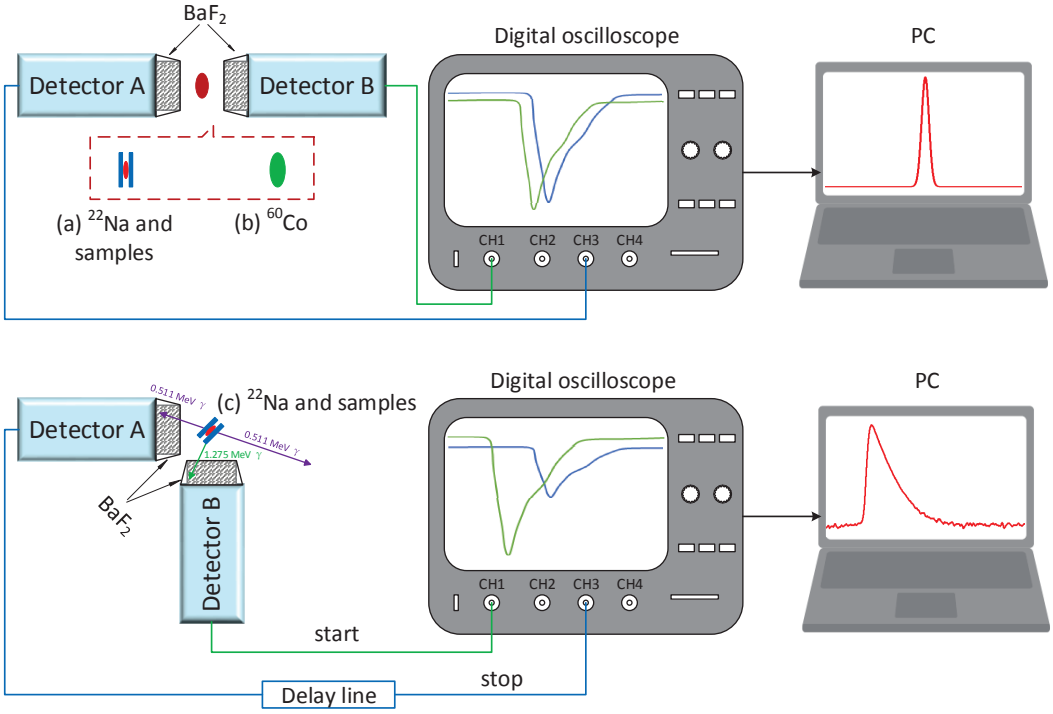

Figure 2. Configuration of CTR measurement systems for (a) the 0.511 MeV annihilation γ-ray pairs, (b) the ^{60}Co cascade γ-rays. (c) Scheme diagram of the digital PAL spectrometer. The purple and green arrows show the trace of 0.511 and 1.275 MeV γ-rays, respectively.

2.3 Digital PAL spectrometer

A new PAL spectrometer consisting of a pair of detectors and a fast digital was developed to carry out PAL experiments. The ^{22}Na source was also used in the PAL experiments as a source of positrons. The 1.275 MeV nuclear γ-ray, emitted immediately following the emission of a positron from ^{22}Na, is regarded as the birth signal of the positron. Two 0.511 MeV annihilation γ-rays (the annihilation signal of the positron) are emitted back-to-back, while the 1.275 MeV nuclear γ-ray is uncorrelated. A schematic diagram of the PAL spectrometer is shown in figure 2 (c). Detector-A (stop detector) was used to detect the 0.511 MeV annihilation γ-rays while detector-B was "start detector", used to detect the 1.275 MeV nuclear γ-rays. The two detectors were placed in a verticle geometry configuration to reduce the pile-up effect [8, 19, 32] in the start detector which can lead to the deterioration of PAL spectra. The pulses from detector-A were delayed for about 5 ns using a coaxial cable. The digital oscilloscope was set to the qualified mode on ch1 and ch3 to accept the pairs of waveforms exceeding the trigger level within a time interval of 50 ns.

As shown in figure 3, a digital PAL event was captured by the oscilloscope. The rise time of the pulses is about 0.9 ns, which is nearly equal to the specific anode pulse rise time of H6610 PMTs (0.7 ns). The waveform data were acquired by the digital oscilloscope operating at a sampling rate of 20 GS/s, namely, the sampling interval was 50 ps. The full-time scale range of input channels was set to 50 ns. Since the waveform data were originated from coincidence events, the PAL spectrum was constructed by histogramming the time interval between the pulses from detector-A and detector-B after pulse discrimination.

2020 JINST 15 P06001

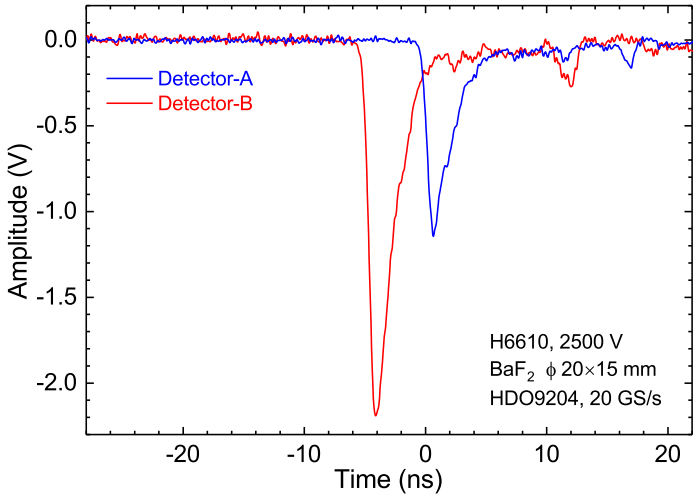

Figure 3. A pair of output pluses from the detectors recorded by the LeCroy HDO9204 oscilloscope. The sampling rate is 20 G/s.

2.4 Pulse discrimination methods

The pulse discrimination was performed to extract suitable pulses for timing analysis, which corresponds to setting the energy windows for start and stop signals in conventional PAL spectrometers. In the experiments, some distorted waveforms with unstable baselines or the pile-up waveforms appeared in the time scale range of one channel, which may lead to the worse performance or wrong results. To choose qualified pulses, the baseline recovery was performed for each pulse, and the pile-up pulses were eliminated by the pulse shape discrimination algorithm.

According to the principle of PMT readout circuits [33], the total integrated charge of the measured pulse is proportional to the sum of the scintillation photons [34], namely, the energy of the detected γ-ray. The total integrated charge of the pulse is proportional to the pulse area between the digitized waveform and its baseline, thus the γ-ray energy can be expressed in terms of the pulse area, which is determined by summing the voltage value at each sampling point over the whole pulse. The energy spectrum (the number of counts as a function of pulse area in terms of channel) of the ^{22}Na γ-rays measured by the digital oscilloscope is shown in figure 4. The counts in low channel numbers (the grey region in figure 4) are decreased as a result of the trigger threshold set in the oscilloscope, which makes no difference to the pulse discrimination, so this part is not shown in figure 4. The FWHM (ΔE) of 511 keV photopeak is about 126.2 keV, namely, the energy resolution ($\Delta E/E_\gamma$) of about 24.7%, which is much worse than the typical energy resolution of BaF_2 detectors in analog systems (about 9 to 13%) [1, 15, 35]. The decay time of the slow scintillation component of BaF_2 crystal (about 620 ns) [2] is too long to be integrated completely in digital measurements, thus contributing to the worse energy resolution. Fortunately, the photopeaks of 0.511 and 1.275 MeV γ-rays with their Compton edges can be distinguished as shown in figure 4, the reconstructed energy spectrum is featured enough to perform the pulse area discrimination in the digital PAL spectrometer, as well as in the CTR measurement systems.

2020 JINST 15 P06001

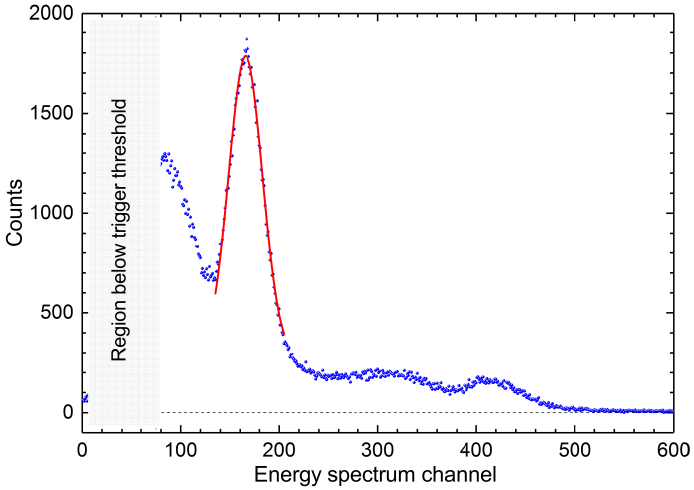

Figure 4. The energy spectrum of ^{22}Na γ-rays measured with a BaF_2-based H6610 scintillation detector. The red line is a Gaussian fitting curve at the photopeak of 0.511 MeV γ-rays.

2.5 Timing analysis methods

There are several algorithms to extract the time information of the pulse, such as leading-edge discrimination, moment-analysis, pulse-shape fitting, and digital constant fraction discrimination (DCFD) [17]. For most scintillation detectors, it is generally believed that the best way to obtain the arrival time of a pulse is DCFD [24, 25, 36]. According to the principle of DCFD, the arrival time of a pulse is defined as the instant when the pulse crosses a threshold fA, where A and f represent the amplitude of the pulse and the constant fraction level, respectively. The optimum constant fraction is a characteristic of the detector depending on the scintillator and PMT types.

The threshold cross time value was obtained using the Gaussian fitting to the leading edge of the pulses. The top 60% of total sampling points in the leading edge of the pulses were used to perform the Gaussian fitting. In the experiments, the time difference between two pulses is calculated as

$$\Delta t^{\mathrm{CFD}} = t_A^{\mathrm{CFD}} - t_B^{\mathrm{CFD}}, \tag{2.1}$$

where t_A^{CFD}, t_B^{CFD} are the DCFD threshold crossing values of a pair of pluses from detector-A and detector-B, respectively.

After the selection of the γ-ray energy, these differences were plotted as a histogram which acts as a time spectrum for ^{60}Co cascade γ-rays or 0.511 MeV annihilation γ-rays. Then we used a Gaussian distribution to fit the time spectrum. The FWHM of the fitted spectrum was used as the CTR of the detectors. For the digtal PAL spectrometer, a PAL spectrum was also constructed by the frequency distribution of Δt^{CFD}, but the time resolution of the PAL spectrometer was extracted by analyzing the PAL spectrum using the MCMC-BI program [37].

3 Results and discussion

As mentioned above, a series of high voltages were applied on the detectors to obtain the optimal time resolution for 0.511 MeV annihilation γ-ray pairs and corresponding constant fraction values.

2020 JINST 15 P06001

The results of the CTR measurements with 0.511 MeV annihilation γ-ray pairs for BaF_2-based H6610 detectors are shown in figures 5, 6, 7, and 8. f_A and f_B represent the constant fraction values for detector-A and detector-B, respectively.

As the high voltage for detector-A is varied from 1800 to 2500 V, the position of the region with minimum FWHM in figure 5 moves towards the side of smaller f_A gradually. The optimal f_A decreases from 0.33 to 0.21 as shown in figure 7 (a), while the optimal f_B remains at around 0.32 as the high voltage for detector-B was kept at 1800 V. As shown in figure 8, the minimum FWHM drops from 196.4 to 182.9 ps. In the condition that the high voltage for detector-A remains at 2500 V and the high voltage for detector-B is increased from 1800 to 2500 V, the region with minimum FWHM in figure 6 has a similar variation rule like that in figure 5, namely, it moves towards the side of smaller f_B. The optimal f_A stays around 0.18 and the optimal f_B falls off from 0.33 to 0.17, as shown in figure 7 (b). The corresponding minimum FWHM is reduced from 182.9 to 161.6 ps. As a result, better FWHM can be obtained at higher voltages for detectors. Therefore, for the limitation of the supply voltage of H6610 PMTs, the optimal CTR of BaF_2-based H6610 detectors for 511 keV annihilation γ-ray pairs is 161.6 ps when the high voltages for detectors are both 2500 V, and the corresponding f values are 0.19 and 0.17, respectively. The difference between the two f values is very small, indicating a good consistency between the two detectors.

For the reference detectors, the CTR of BaF_2-based H3378 detectors for 511 keV annihilation γ-ray pairs for was also investigated. As shown in table 2, the optimal supply voltages for the reference detectors are both 3400 V, the optimal f_A and f_B are 0.23 and 0.21, respectively. The best FWHM is about 171 ps, slightly worse than that of BaF_2-based H6610 detectors. These CTR values are comparable with the typical values in analog systems (160–180 ps) [35, 38].

The time responses of the detectors at the optimal supply voltages for the ^{60}Co cascade radiations are listed in table 3. The best FWHM of BaF_2-based H6610 detectors is 108 ps, much better than that of BaF_2-based H3378 detectors (122 ps). The energy range is set to $1.0 < E < 1.5$ MeV.

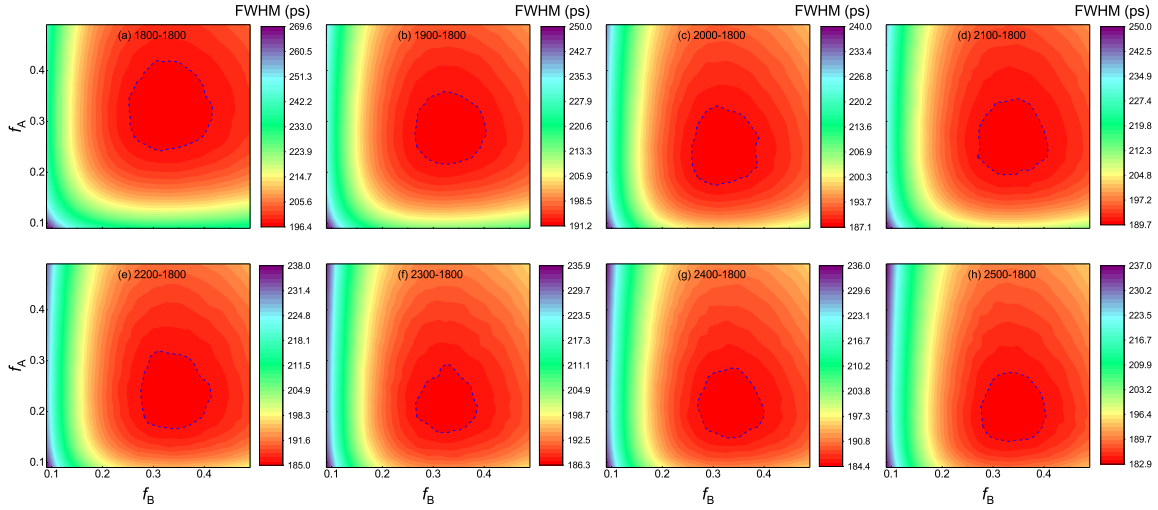

Figure 5. The CTR of BaF_2-based H6610 detectors as a function of f_B for detector-B at the supply voltage of 1800 V and f_A for detector-A at the supply voltage of (a) 1800 V, (b) 1900 V, (c) 2000 V, (d) 2100 V, (e) 2200 V, (f) 2300 V, (g) 2400 V, (h) 2500 V. The dash contour lines are guides for the eyes.

2020 JINST 15 P06001

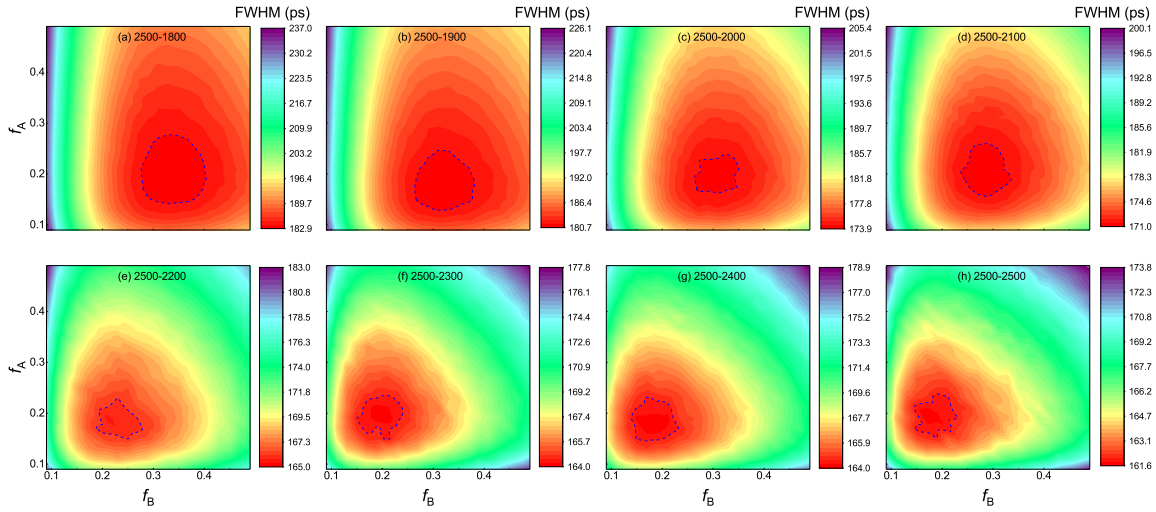

Figure 6. The CTR of BaF_2-based H6610 detectors as a function of f_A for detector-A at the supply voltage of 2500 V and f_B for detector-B at the supply voltage of (a) 1800 V, (b) 1900 V, (c) 2000 V, (d) 2100 V, (e) 2200 V, (f) 2300 V, (g) 2400 V, (h) 2500 V. The dash contour lines are guides for the eyes.

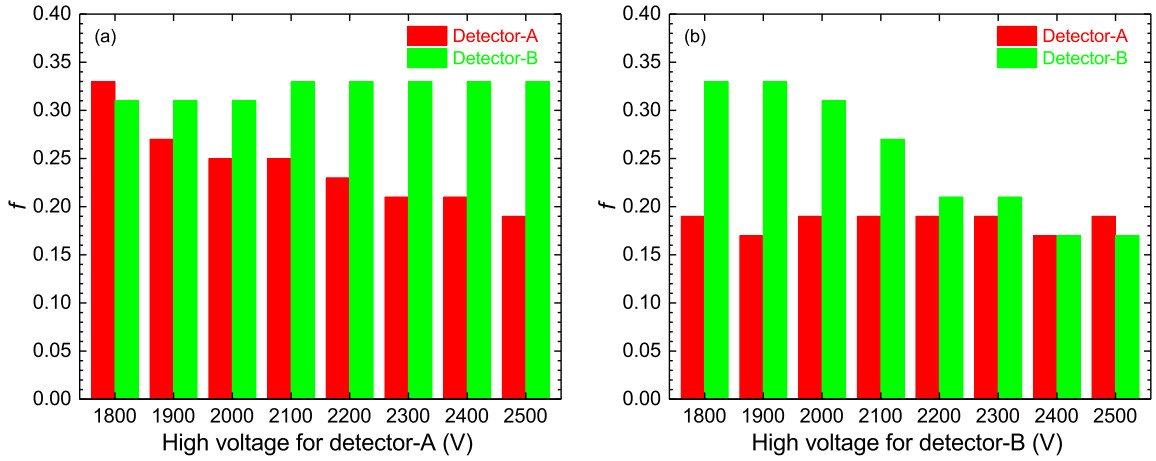

Figure 7. The optimal constant fraction as a function of the supply voltage for (a) detector-A when the supply voltage for detector-B is 1800 V, (b) detector-B when the supply voltage for detector-A is 2500 V.

Table 2. The CTR of the detectors measured with 0.511 MeV annihilation γ-ray pairs.

γ-ray source	γ-ray energy (MeV)	PMT	High voltage (V)	Energy window (MeV)	Sampling rate (GS/s)	f_A	f_B	FWHM (ps)
^{22}Na	0.511	H6610	2500	$0.3 < E < 0.6$	20	0.19	0.17	162
^{22}Na	0.511	H3378	3400	$0.3 < E < 0.6$	20	0.23	0.21	171

2020 JINST 15 P06001

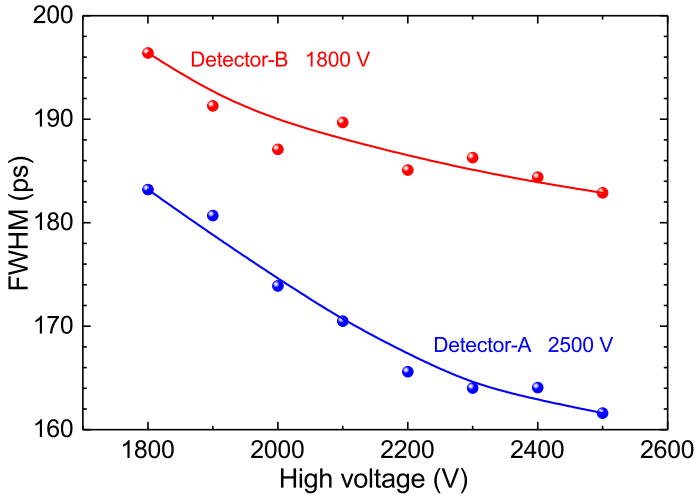

Figure 8. The time resolution as a function of the supply voltage. The red (blue) dots represent the variation of FWHM with supply voltage for detector-A (detector-B) when the supply voltage for detector-B (detector-A) is 1800 V (2500 V).

The corresponding f_A and f_B are both 0.15 for the BaF_2-based H6610 detectors, while the values are 0.17 and 0.13 for BaF_2-based H3378 detectors, respectively. Compared to the f_A and f_B for the 0.511 MeV γ-rays, the values for 1.17 and 1.33 MeV γ-rays are decreased obviously, which is attributed to the larger pulse amplitude for higher energy of γ-rays. Therefore, the constant fraction values for 0.511 and 1.275 MeV γ-rays are different in the digital PAL spectrometer.

Table 3. The CTR of the detectors measured with ^{60}Co cascade γ-rays.

γ-ray source	γ-ray energy (MeV)	PMT	Energy window (MeV)	Sampling rate (GS/s)	f_A	f_B	FWHM (ps)
^{60}Co	1.17, 1.33	H6610	$1.0 < E < 1.5$	20	0.15	0.15	108
^{60}Co	1.17, 1.33	H3378	$1.0 < E < 1.5$	20	0.17	0.13	122

To investigate the influence of the sampling rate of the oscilloscope on the CTR, time spectra for the ^{60}Co cascade radiations were measured with different sampling rates (2.5–40 GS/s). The lower sampling rate was not applied in the experiments, considering that at a low sampling rate, the number of sampling points in the leading edge of the pulse is not enough to implement timing analysis. The CTR as a function of the sampling rate is shown in figure 9. The CTR of BaF_2-based H6610 detectors displays a rapid decline at the sampling rate increasing from 2.5 to 10 GS/s and is improved by about 12 ps as shown in figure 9 (a). However, the time resolution at 40 GS/s becomes only 4 ps better than that at 10 GS/s. In figure 9 (b), the time resolution of BaF_2-based H3378 detectors shows a similar variation, namely, it is improved by about 12 ps at the sampling rate from 2.5 to 10 GS/s, and only 3 ps from 10 to 40 GS/s. The results indicate that a low sampling rate has much influence on the timing accuracy, thus worsening the time resolution. So higher sampling rate should be adopted in the experiments when possible.

2020 JINST 15 P06001

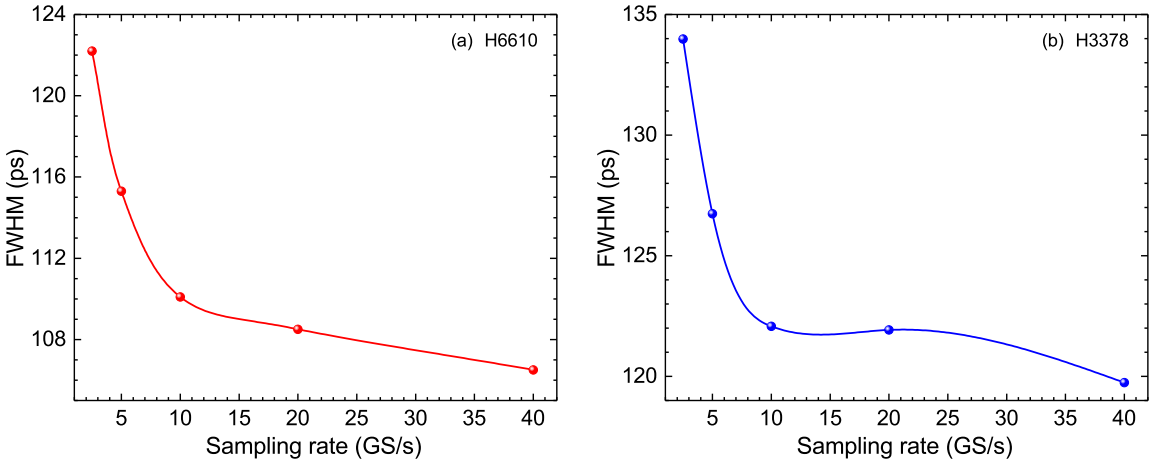

Figure 9. The time resolution as a function of the sampling rate for (a) BaF_2-based H6610 detectors, (b) BaF_2-based H3378 detectors.

Positron annihilation lifetime spectra for yttria-stabilized zirconia (YSZ) samples were measured to investigate the performance of the digital PAL spectrometer. The 9 mol % Y_2O_3 doped YSZ samples (from Hefei Kejing Materials Technology Co., Ltd.) were used as reference samples for its single positron lifetime component of about 180 ps [39, 40]. It took about 10 hours to accumulate 3×10^6 counts for each spectrum with a ^{22}Na source of about 0.37 MBq. All of the spectra were analyzed by the MCMC-BI program. The settings of the digital PAL spectrometer and results of PAL spectra for YSZ are listed in table 4. It should be noted that wide energy windows were applied to ensure a high count rate. For the spectrometer composed of BaF_2-based H6610 detectors, the YSZ spectrum resulted in a time resolution of 130.1 ps with two lifetime components τ_1 and τ_2. τ_1 (181.5 ps) is attributed to free positrons in YSZ samples, and τ_2 (550 ps) is due to the source components. Posterior constraints of all five parameters near the optimal solution for the YSZ spectrum calculated by the MCMC-BI method are also shown in figure 10. These curves display clearly the location of all optima and the types of distributions. As a reference spectrometer, the spectrometer composed of BaF_2-based H3378 detectors also measured a PAL spectrum for YSZ. The spectrum yields a time resolution of 138.3 ps with the fitted lifetime τ_1 (178.8 ps) in YSZ samples. Both of the fitted lifetimes in YSZ samples are consistent with previous works [39, 40]. The comparison of the two spectra indicate that the spectrometer composed of BaF_2-based H6610 detectors has a better time performance than that of BaF_2-based H3378 detectors.

The time resolution of a PAL spectrometer is crucial to resolve accurate positron lifetime components from a spectrum. The time resolution values of existing digital PAL spectrometers are still higher than the positron lifetimes in some defect-free metals [41] or semiconductors [42] (100–140 ps), or just comparable with these lifetimes. Therefore, it's still of great importance for any improvements in time resolution when investigating positron annihilation in meals or semiconductors. In the next step, we will apply more BaF_2-based H6610 detectors in our positron annihilation lifetime experiments. The symmetrical PAL spectrometers [43] composed of BaF_2-based H6610 detectors would also be considered.

2020 JINST 15 P06001

Table 4. The settings of the digital PAL spectrometer and results of PAL spectra for YSZ fitted by the MCMC-BI program (posterior mean results).

Detector	BaF_2-based H6610 detector	BaF_2-based H3378 detector
High voltage (V)	2500	3400
Sampling rate (GS/s)	20	20
Energy window (MeV)	$0.3 < E < 0.6$	$0.3 < E < 0.6$
	$1.0 < E < 1.5$	$1.0 < E < 1.5$
f_A	0.19	0.23
f_B	0.15	0.13
τ_1 (ps)	181.5	178.8
FWHM (ps)	130.1	138.3

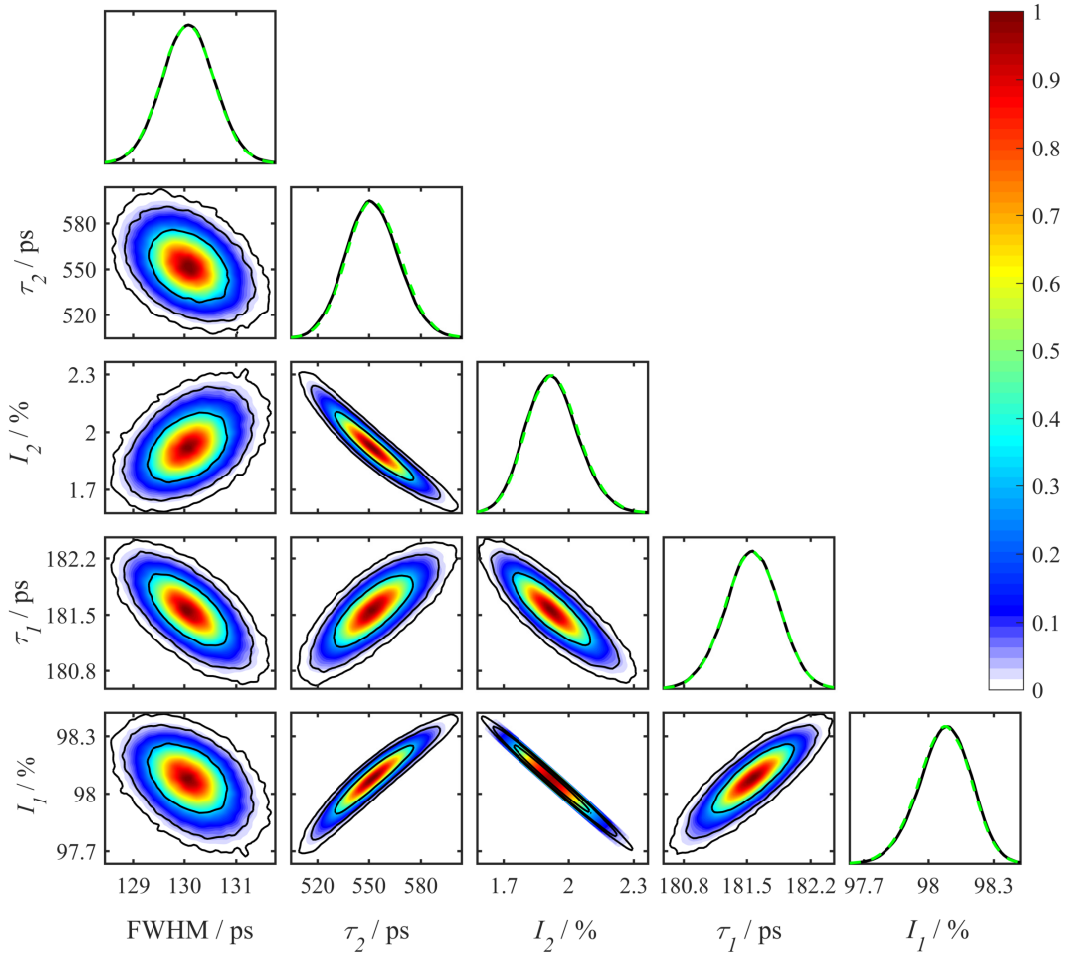

Figure 10. Posterior constraints of all five parameters near the optimal solution for YSZ spectrum calculated by the MCMC-BI method.

4 Conclusions

In this work, the time performance of BaF_2-based H6610 detectors was investigated using a digital oscilloscope. The effects of high voltages and digital constant fraction values for detectors were taken into account. The CTR values for 0.511 MeV annihilation γ-ray pairs and ^{60}Co cascade γ-rays are 162 and 108 ps, respectively. A new digital PAL spectrometer composed of two BaF_2-based H6610 detectors and an oscilloscope was developed with a time resolution of about 130 ps, better than that composed of BaF_2-based H3378 detectors. This work extends the applications of BaF_2-based H6610 detectors to the areas requiring fast timing, espcially PAL spectroscopy.

Acknowledgments

This work was supported by the National Key R&D Program of China (Grant No. 2019YFA0210000) and the National Natural Science Foundation of China (Grant Nos. 11775215, 11875248, and 11975225).

References

[1] M. Laval et al., *Barium fluoride — Inorganic scintillator for subnanosecond timing*, *Nucl. Instrum. Meth.* **206** (1983) 169.

[2] P. Lecoq, A. Gektin and M. Korzhik, *Inorganic scintillators for detector systems: physical principles and crystal engineering*, Springer-Verlag, Berlin, Heidelberg (2006).

[3] W. Wong, N.A. Mullani, G. Wardworth, R.K. Hartz and D. Bristow, *Characteristics of Small Barium Fluoride (BaF_2) Scintillator for High Intrinsic Resolution Time-of-Flight Positron Emission Tomography*, *IEEE Trans. Nucl. Sci.* **31** (1984) 381.

[4] C. Hu et al., *BaF_2 : Y and ZnO : Ga crystal scintillators for GHz hard X-ray imaging*, *Nucl. Instrum. Meth.* **A 950** (2020) 162767.

[5] D.-L. Zhang et al., *System design for precise digitization and readout of the CSNS-WNS BaF_2 spectrometer*, *Chin. Phys.* **C 41** (2017) 026102.

[6] S.J. Williams et al., *Testing the integration of BaF_2 detectors into the 8π array: Fast-timing measurements at TRIUMF*, *J. Phys.* **G 31** (2005) S1979.

[7] T.B. Chang et al., *Improvement on application of BaF_2 scintillation counter to a positron lifetime spectrometer*, *Nucl. Instrum. Meth.* **256** (1987) 398.

[8] H. Rajainmäki, *High-resolution positron lifetime spectrometer with BaF_2 scintillators*, *Appl. Phys.* **A 42** (1987) 205.

[9] F. Tuomisto and I. Makkonen, *Defect identification in semiconductors with positron annihilation: Experiment and theory*, *Rev. Mod. Phys.* **85** (2013) 1583.

[10] J. Čížek, *Characterization of lattice defects in metallic materials by positron annihilation spectroscopy: A review*, *J. Mater. Sci. Technol.* **34** (2018) 577.

[11] P. Rajesh et al., *Positron Annihilation Studies on Chemically Synthesized FeCo Alloy*, *Sci. Rep.* **8** (2018) 9764.

[12] R.L. Garwin, *Thermalization of Positrons in Metals*, *Phys. Rev.* **91** (1953) 1571.

2020 JINST 15 P06001

[13] W. Brandt, S. Berko and W.W. Walker, *Positronium Decay in Molecular Substances*, *Phys. Rev.* **120** (1961) 1864.

[14] M. Eldrup, D. Lightbody and J.N. Sherwood, *The temperature dependence of positron lifetimes in solid pivalic acid*, *Chem. Phys.* **63** (1981) 51.

[15] F. Bečvář, J. Čížek, L. Lešták, I. Novotný, I. Procházka and F. Šebesta, *A high-resolution BaF_2 positron-lifetime spectrometer and experience with its long-term exploitation*, *Nucl. Instrum. Meth.* **A 443** (2000) 557.

[16] H. Saito, Y. Nagashima, T. Kurihara and T. Hyodo, *A new positron lifetime spectrometer using a fast digital oscilloscope and BaF_2 scintillators*, *Nucl. Instrum. Meth.* **A 487** (2002) 612.

[17] M.A. Nelson, B.D. Rooney, D.R. Dinwiddie and G.S. Brunson, *Analysis of digital timing methods with BaF_2 scintillators*, *Nucl. Instrum. Meth.* **A 505** (2003) 324.

[18] L. Wei, Z.M. Zhang, C.X. Ma, C.L. Zhou, B.Y. Wang and T.B. Chang, *A high-resolution BaF_2 positron lifetime spectrometer with high counting rate*, *Mater. Sci. Forum* **445-446** (2004) 416.

[19] H. Saito and T. Hyodo, *Direct Measurement of the Parapositronium Lifetime in α-SiO_2*, *Phys. Rev. Lett.* **90** (2003) 193401.

[20] M. Jardin, M. Lambrecht, A. Rempel, Y. Nagai, E. van Walle and A. Almazouzi, *Digital positron lifetime spectrometer for measurements of radioactive materials*, *Nucl. Instrum. Meth.* **A 568** (2006) 716.

[21] K. Rytsölä, J. Nissilä, J. Kokkonen, A. Laakso, R. Aavikko and K. Saarinen, *Digital measurement of positron lifetime*, *Appl. Surf. Sci.* **194** (2002) 260.

[22] F. Bečvář, *Digital positron lifetime spectroscopy: present status and outlook*, *Phys. Status Solidi* **C 4** (2007) 3939.

[23] K. Ito et al., *Interlaboratory comparison of positron annihilation lifetime measurements for synthetic fused silica and polycarbonate*, *J. Appl. Phys.* **104** (2008) 0261021.

[24] H. Li, Y.D. Shao, K. Zhou, J.B. Pang, Z. Wang, *A simplified digital positron lifetime spectrometer based on a fast digital oscilloscope*, *Nucl. Instrum. Meth.* **A 625** (2011) 29.

[25] R. An, B. Chen, Y.F. Yan, B.J. Ye, W. Kong and S. Ritt, *A new positron annihilation lifetime spectrometer based on DRS4 waveform digitizing board*, *Chin. Phys.* **C 38** (2014) 056001.

[26] H.B. Wang, Q.H. Zhao, H. Liang, B.C. Gu, J.D. Liu, H.J. Zhang and B.J. Ye, *A new SiPM-based positron annihilation lifetime spectrometer using LYSO and LFS-3 scintillators*, *Nucl. Instrum. Meth.* **A 960** (2020) 163662.

[27] Hamamatsu Photonics K.K., *Photomultiplier Tube Assemblies*, https://www.hamamatsu.com/resources/pdf/etd/PMT_76-83_en.pdf.

[28] Hamamatsu Photonics K.K., *Hamamatsu H6610 datasheet*, http://dtsheet.com/doc/749739/hamamatsu-h6610.

[29] Hamamatsu Photonics K.K., *Hamamatsu R2083 datasheet*, https://www.hamamatsu.com/resources/pdf/etd/R2083_R3377_TPMH1227E.pdf.

[30] *ROOT webpage*, https://root.cern.ch/.

[31] *GNU Scientific Library webpage*, https://www.gnu.org/software/gsl/.

[32] L.H. Cong et al., *Reconfigurable positron annihilation lifetime spectrometer utilizing a multi-channel digitizer*, *Nucl. Instrum. Meth.* **A 946** (2019) 162691.

2020 JINST 15 P06001

[33] Hamamatsu Photonics K.K., *Photomultiplier Tubes: Basics and Applications*, Edition 3a (2007).

[34] P.A. Söderström, J. Nyberg and R. Wolters, *Digital pulse-shape discrimination of fast neutrons and γ rays*, *Nucl. Instrum. Meth.* **A 594** (2008) 79 [arXiv:0805.0692].

[35] U. Ackermann, W. Egger, P. Sperr and G. Dollinger, *Time- and energy-resolution measurements of BaF_2, BC-418, LYSO and $CeBr_3$ scintillators*, *Nucl. Instrum. Meth.* **A 786** (2015) 5.

[36] J. Nissilä, K. Rytsölä, R. Aavikko, A. Laakso, K. Saarinen and P. Hautojärvi, *Performance analysis of a digital positron lifetime spectrometer*, *Nucl. Instrum. Meth.* **A 538** (2005) 778.

[37] B.C. Gu, W.S. Zhang, J.D. Liu, H.J. Zhang and B.J. Ye, *Accurate and informative analysis of positron annihilation lifetime spectra by using Markov Chain Monte-Carlo Bayesian inference method*, *Nucl. Instrum. Meth.* **A 928** (2019) 37.

[38] N. Satoh, K. Shimizu, H. Uchida, T. Yamashita and E. Tanaka, *A time-of-flight multi-probe system for positron imaging*, *IEEE Trans. Nucl. Sci.* **43** (1996) 1921.

[39] X. Guo and Z. Wang, *Effect of niobia on the defect structure of yttria-stabilized zirconia*, *J. Eur. Ceram. Soc.* **18** (1998) 273.

[40] O. Melikhova et al., *Positron annihilation in three zirconia polymorphs*, *Phys. Status Solidi* **C 4** (2007) 3831.

[41] J.M. Campillo Robles and F. Plazaola, *Collection of Data on Positron Lifetimes and Vacancy Formation Energies of the Elements of the Periodic Table*, *Defect Diffus. Forum* **213-215** (2003) 141.

[42] A. Kawasuso et al., *Silicon vacancies in 3C-SiC observed by positron lifetime and electron spin resonance*, *Appl. Phys.* **A 67** (1998) 209.

[43] N. Djourelov, N. Charvin, C. Bas, J. Viret, V. Samoylenko and D. Sillou, *Symmetric analog positron lifetime spectrometer utilizing charge-to-digital converters*, *Nucl. Instrum. Meth.* **B 264** (2007) 165.

2020 JINST 15 P06001